

Spectral decomposition of starbursts and AGNs in 5–8 μm *Spitzer* IRS spectra of local ULIRGs

E. Nardini,¹ G. Risaliti,^{2,3} M. Salvati,² E. Sani,¹
M. Imanishi,⁴ A. Marconi¹ and R. Maiolino⁵

¹ *Dipartimento di Astronomia, Università di Firenze, L.go E. Fermi 2, 50125 Firenze, Italy. E-mail: nardini@arcetri.astro.it*

² *INAF - Osservatorio Astrofisico di Arcetri, L.go E. Fermi 5, 50125 Firenze, Italy*

³ *Harvard-Smithsonian Center for Astrophysics, 60 Garden St. Cambridge, MA 02138 USA*

⁴ *National Astronomical Observatory, 2-21-1, Osawa, Mitaka, Tokyo 181-8588, Japan*

⁵ *INAF - Osservatorio Astronomico di Roma, via di Frascati 33, 00040 Monte Porzio Catone (RM), Italy*

Released XXXX XXXXX XX

ABSTRACT

We present an analysis of the 5–8 μm *Spitzer*-IRS spectra of a sample of 68 local Ultraluminous Infrared Galaxies (ULIRGs). Our diagnostic technique allows a clear separation of the active galactic nucleus (AGN) and starburst (SB) components in the observed mid-IR emission, and a simple analytic model provides a *quantitative* estimate of the AGN/starburst contribution to the bolometric luminosity. We show that AGNs are ~ 30 times brighter at 6 μm than starbursts with the same bolometric luminosity, so that even faint AGNs can be detected. Star formation events are confirmed as the dominant power source for extreme infrared activity, since $\sim 85\%$ of ULIRG luminosity arises from the SB component. Nonetheless an AGN is present in the majority (46/68) of our sources.

Key words: galaxies: active; galaxies: starburst; infrared: galaxies.

1 INTRODUCTION

Ultraluminous Infrared Galaxies (ULIRGs, $L_{\text{IR}} > 10^{12} L_{\odot}$) are the local counterparts of the high-redshift objects dominating the cosmic background in the far-infrared and millimetric bands. Unveiling the nature of their energy source is fundamental in order to understand the star formation history and the obscured AGN activity in the distant Universe.

Since their discovery, several infrared indicators have been proposed to determine whether the central engine in ULIRGs is an AGN or a starburst (SB). The presence of high-ionization lines in the mid-IR spectra of ULIRGs points to AGN activity, while intense PAH emission features are typical of starburst environments (Genzel et al. 1998; Laurent et al. 2000). Recently, the absorption feature of amorphous silicate grains centered at 9.7 μm has also been used together with the PAH emission to assess the nature of the obscured power source (Spoon et al. 2007). An alternate way to disentangle AGNs and SBs in ULIRGs has been proposed by Risaliti et al. (2006, hereafter R06), based on the separation of the two continuum components in 3–4 μm spectra. This method has been successfully applied to a sample of ~ 50 nearby ULIRGs (Risaliti, Imanishi & Sani 2007, *submitted*) and provided an estimate of the average AGN/SB contribution to ULIRGs. The key reason for using the continuum emission at $\lambda \simeq 3\text{--}4 \mu\text{m}$ as a diagnostic is the differ-

ence between the 3- μm to bolometric ratios in AGNs and starbursts (\sim two orders of magnitude larger in the former). This makes the detection of the AGN component possible even when the AGN is heavily obscured and/or bolometrically weak compared to the starburst. However the original prescription is limited by the low quality of the available L-band spectra of ULIRGs (R06, Imanishi et al. 2006), which makes the results on individual sources highly uncertain, except for the $\sim 10\text{--}15$ brightest objects.

At present we have extended the analysis to the 5–8 μm spectral band, using the observations of the IRS instrument (Houck et al. 2004) onboard *Spitzer*. We disentangled the AGN and SB contributions to the observed 5–8 μm emission of ULIRGs by combining average spectral templates representing the different properties of the two physical processes at work. The high quality of *Spitzer*-IRS data, in addition to the relatively low dispersion of the intrinsic continuum properties of both AGNs and starbursts in this spectral range, allows a much more accurate determination of the AGN/SB components than possible at other wavelengths (e.g. X-rays) or with other diagnostic methods based on emission lines. In this paper we present our decomposition method, and discuss a simple analytical model providing a *quantitative* estimate of the AGN/SB contribution to the bolometric luminosity of each source.

2 OBSERVATIONS AND DATA REDUCTION

In order to perform a detailed study of a representative sample of ULIRGs in the local Universe, we selected 68 sources with $z < 0.15$ and a $60\text{-}\mu\text{m}$ flux density $f_{60} > 1$ Jy. Most of the objects are taken from the IRAS ULIRG 1 Jy sample (Kim & Sanders 1998), but a few more sources in the southern hemisphere have also been included. The flux limit at $60\text{ }\mu\text{m}$ ensures an unbiased selection with respect to the relative AGN/SB contributions.

IRS observations were obtained within three different programs: PID 105 (PI J.R.Houck), PID 2306 (PI M.Imanishi), PID 3187 (PI S.Veilleux). The coadded images provided by the *Spitzer Science Center* (after the treatment with pipeline version S13.0) have been background-subtracted by differencing the two observations in the nodding cycle. The spectra have been extracted and calibrated following the standard procedure for point-like sources with the package *SPICE*. The flux uncertainties have been estimated from source and background counts (in e^-/s). Finally, we performed a smooth connection between the Short-Low spectral orders, with no necessity of relative scaling.

Out of the 68 spectra, we already published 48 in Imanishi et al. 2007. Six more spectra are shown in Armus et al. 2006, 2007. The remaining 14 spectra are analyzed here for the first time and will be fully presented in a forthcoming paper (Nardini et al. 2008, *in prep.*).

3 THE 5–8 μm AGN/SB SEPARATION

Despite the diversity of the global IRS spectra of pure AGNs and pure SBs, and the complexity of the physics involved, little dispersion is seen at wavelengths shortward of the $9.7\text{ }\mu\text{m}$ silicate feature. This makes possible the use of universal AGN/SB templates to reproduce the spectral properties of ULIRGs in the 5–8 μm interval. In the following we describe the templates adopted in our model.

Starburst. The mid-IR spectral features of local SB galaxies show very little variations from one object to another in the 5–8 μm wavelength range, while larger differences are present in the $\sim 9\text{--}30\text{ }\mu\text{m}$ band (Brandl et al. 2006, hereafter B06). In order to check if this is the case in the ULIRG luminosity range as well, we analyzed the sources in our sample established to be starburst-dominated by multi-band studies. We did not find significant variations among the spectra, concluding that a fixed template can be used to represent the 5–8 μm SB component in local ULIRGs. We built such template using the five brightest objects among the pure SBs in our sample (IRAS 10190+1322, IRAS 12112+0305, IRAS 17208–0014, IRAS 20414–1651 and IRAS 22491–1808), whose underlying continuum has been reproduced by a power law and normalized at $6\text{ }\mu\text{m}$ before adding. Our SB template is shown in Fig.1, together with its dispersion in the whole IRS spectral band and the B06 template. The little spectral dispersion below $8\text{ }\mu\text{m}$ among SBs of different luminosity (to be compared with their large differences at longer wavelengths) is in itself an interesting result, which should be fully investigated through detailed emission and radiative transfer models. Concerning this we only notice that such a remarkable similarity can result from the spatial integration over a large number of individual star-forming regions.

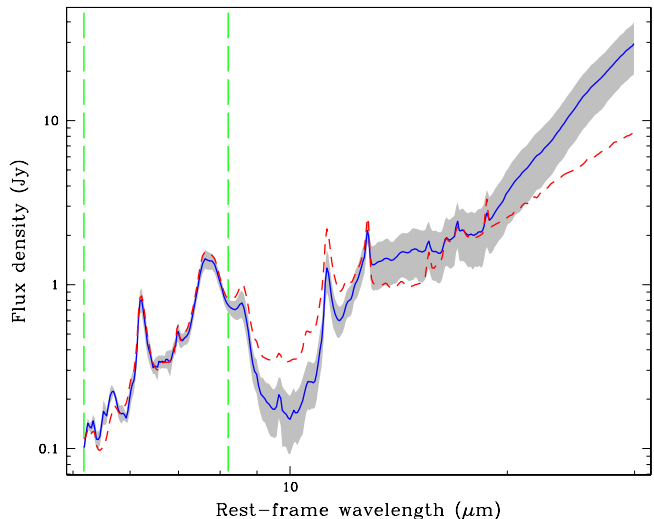


Figure 1. Comparison between the SB template of B06 (dashed red line) and our template (solid blue line), constructed from the emission of the 5 brightest SB-dominated ULIRGs. The shaded area shows the $1\text{-}\sigma$ rms dispersion in the 5 ULIRG spectra. The vertical long-dashed green lines enclose the fitting region.

AGN. Our recent L-band analysis of bright ULIRGs shows that the intrinsic AGN emission is due to hot dust grains and the flux density is well described by a featureless power law with a fixed spectral index: $f_\nu \propto \lambda^{1.5}$. Here we adopt the same spectral shape up to $8\text{ }\mu\text{m}$, in agreement with new *Spitzer* observations of a large sample of local type 1 quasars (Netzer et al. 2007).

An active nucleus is much more compact than a circumnuclear starburst region. As a consequence, the near-IR radiation due to thin dust reprocessing can be itself strongly reddened because of a compact absorber along the line of sight. We therefore introduce an exponential attenuation factor $e^{-\tau(\lambda)}$, where the optical depth follows the conventional law $\tau(\lambda) \propto \lambda^{-1.75}$ (Draine 1989). A similar correction is not needed in the SB template. We stress that this does not imply that the starburst spectrum is not affected by inner obscuration; the possible effects of this obscuration (which are clear at longer wavelengths, e.g. in the silicate absorption features at 9.7 and $\sim 18\text{ }\mu\text{m}$) are however already accounted for in the adopted observational template.

Summarizing, the different contributions to the observed energy output of a ULIRG can be parametrized as follows:

$$f_\nu^{obs}(\lambda) = f_6^{int} [(1 - \alpha_6)u_\nu^{sb} + \alpha_6 u_\nu^{agn} e^{-\tau(\lambda)}] \quad (1)$$

where α_6 is the AGN contribution to the 5–8 μm intrinsic flux density f_6^{int} , while u_ν^{sb} and u_ν^{agn} are the SB and AGN templates normalized at $6\text{ }\mu\text{m}$. Apart from the flux normalization, our model contains only two free parameters, i.e. α_6 and the optical depth to the AGN $\tau(6\text{ }\mu\text{m})$. They are both shown in Tab.1.

Additional high-ionization emission lines and molecular absorption features (due to ices and aliphatic hydrocarbons), whenever present, were fitted by means of gaussian profiles except for the water ice absorption at $\sim 6\text{ }\mu\text{m}$, reproduced with the laboratory profile from the Leiden database corresponding to pure H_2O ice at 30 K .

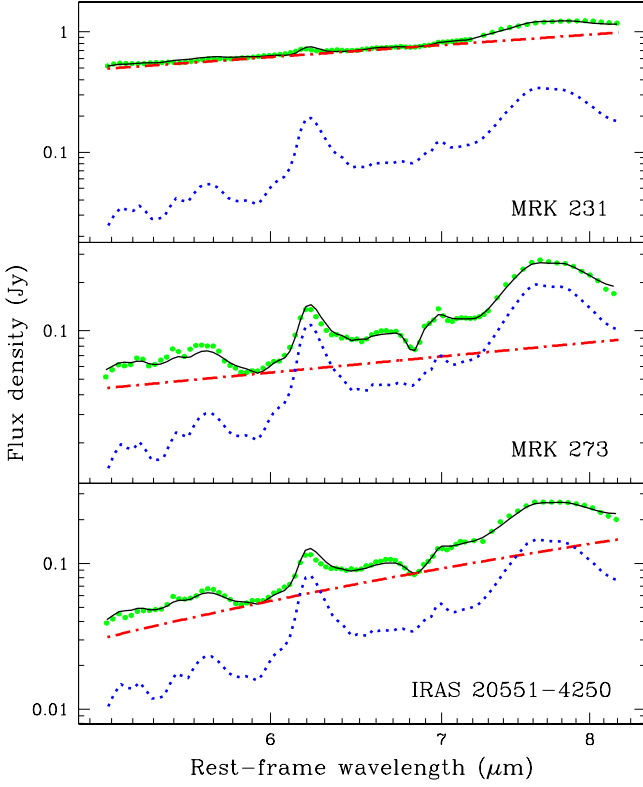


Figure 2. Three representative examples of the typical 5–8 μm spectral shapes of ULIRGs. The differences among the spectra are entirely due to the different AGN contribution and its obscuration. Whenever the AGN is the dominant power source, as in Mrk 231, a strong continuum almost obliterates the PAH features. On the contrary, in Mrk 273 the AGN is fainter and the spectral outline of a starburst is clearly identified. A similar spectrum is exhibited by IRAS 20551–4250, but the features are less prominent and the continuum is steeper: this source harbours an obscured AGN. In each panel, in addition to the data (green filled circles) and their best fits (black thin line), we have included the reddened AGN (red dot-dashed line) and starburst (blue dotted line) components.

Fig.2 shows the spectral decomposition of three representative ULIRGs. In spite of the great diversity of the observed spectra, our simple model provides a good fit of each spectrum in the sample: the residuals from the best fits are in all sources smaller than 10% at all wavelengths (though the fits are not formally acceptable in a statistical sense, with a reduced $\chi^2 \gtrsim 2$, due to the small error bars and the remaining unfitted minor features). In particular, both the PAH emission and the continuum are always well reproduced: this implies that the large variations in the 5–8 μm spectral shape of ULIRGs are entirely due to the AGN contribution and its obscuration. A detailed analysis of the results for each source and a physical interpretation of peculiar cases are the subject of a forthcoming paper (Nardini et al. 2008, *in prep.*).

4 AGN/SB BOLOMETRIC CONTRIBUTIONS

The large difference between the 5–8 μm to bolometric ratios in AGNs and SBs implies that this ratio is itself an indicator

of AGN activity, and can be used (a) to test the consistency of our decomposition method and (b) to estimate the relative AGN and SB contributions to the bolometric luminosity of our sample. We define the 6- μm to bolometric ratio as:

$$R = \left(\frac{\nu_6 f_6^{\text{int}}}{F_{\text{IR}}} \right). \quad (2)$$

where F_{IR} is the total infrared flux, estimated as in Sanders & Mirabel (1996). Since the integrated infrared luminosity of ULIRGs coincides almost exactly with their bolometric luminosity, R is a fair approximation to the fraction of the total energy output that is intrinsically emitted in the 5–8 μm range. Reminding that the intrinsic AGN/SB contributions are $\alpha_6 f_6^{\text{int}}$ and $(1 - \alpha_6) f_6^{\text{int}}$ respectively, and decomposing F_{IR} as $F_{\text{IR}}^{\text{agn}} + F_{\text{IR}}^{\text{sb}}$, a simple connection between R and α_6 is brought out:

$$R = \frac{R^{\text{agn}} R^{\text{sb}}}{\alpha_6 R^{\text{sb}} + (1 - \alpha_6) R^{\text{agn}}}, \quad (3)$$

provided that R^{agn} and R^{sb} , the equivalents of R for pure (unobscured) AGNs and pure SBs, are defined as in Eq.2. We fitted the theoretical $R(\alpha_6)$ relation (Eq.3) to our data considering R^{agn} and R^{sb} as free parameters, and found:

$$\log R^{\text{agn}} = -0.49_{-0.13}^{+0.12} \quad \text{and} \quad \log R^{\text{sb}} = -1.93_{-0.03}^{+0.03}. \quad (4)$$

We note that R^{agn} turns out to be somewhat higher than traditional estimates based on AGN spectral energy distributions: for example, we derive $\log R^{\text{agn}} \sim -0.6$ from the SED of Elvis et al. (1994). This suggests that the local quasars (mostly PG quasars) used to build the mentioned SED can be contaminated to some extent by a starburst contribution, in agreement with recent studies (Netzer et al. 2007).

According to Eq.4, AGNs are ~ 30 times more luminous at 6 μm than starbursts with the same bolometric luminosity. We are now able to quantify the AGN contribution ($\alpha_{\text{bol}} = F_{\text{IR}}^{\text{agn}} / F_{\text{IR}}$) to the total infrared luminosity of each source:

$$\alpha_{\text{bol}} = \frac{\alpha_6}{\alpha_6 + (R^{\text{agn}}/R^{\text{sb}})(1 - \alpha_6)}, \quad (5)$$

where $R^{\text{agn}}/R^{\text{sb}} \simeq 28$. The values of α_{bol} are listed in Tab.1. Our estimates for the ~ 15 brightest sources are in good agreement with those of R06 and with the Genzel et al. (1998) and Laurent et al. (2000) mid-IR diagnostic diagrams. Considering the whole sample, our results can be compared with the optical classification and with L-band and hard X-ray studies, when available. A substantial agreement is obtained in all cases. It is worth noticing that the optical classification alone gives incomplete information: all the sources classified as Seyferts show clear traces of AGN activity, but 7 out of 8 among the ULIRGs with $\alpha_{\text{bol}} > 0.25$ and $\tau > 1$ are indeed classified as LINERs or H II regions. LINERs are again confirmed to be rather heterogeneous with respect to the nature of their energy source. Such ambiguities can be solved by applying our diagnostic.

By inverting Eq.5 the relation between R and α_{bol} takes the neat form $R = \alpha_{\text{bol}} R^{\text{agn}} + (1 - \alpha_{\text{bol}}) R^{\text{sb}}$, and is plotted in Fig.3a. As a final check we have computed for each source the following quantities:

$$\hat{R}^{\text{agn}} = \left(\frac{\nu_6 \alpha_6 f_6^{\text{int}}}{\alpha_{\text{bol}} F_{\text{IR}}} \right) \quad \text{and} \quad \hat{R}^{\text{sb}} = \left[\frac{\nu_6 (1 - \alpha_6) f_6^{\text{int}}}{(1 - \alpha_{\text{bol}}) F_{\text{IR}}} \right]. \quad (6)$$

Table 1. Spectral parameters for the 68 sources in our sample. α_6 : AGN contribution to the intrinsic continuum emission at 6 μm (in percent). τ : Optical depth of the AGN component at 6 μm (we assume $\tau = 0$ for the sources with no detected AGN). α_{bol} : AGN contribution to the bolometric luminosity (in percent). The errors in α_{bol} are due to the statistical uncertainty both in the flux amplitude of the AGN/SB components and in the ratios R^{agn} and R^{sb} . The systematic effects are discussed in the text. *O/X/L*: SB/AGN/LINER classification based on optical, X-ray and L-band spectroscopy. A: AGN, L: LINER, A*: AGN, tentative detection. References: ¹: Veilleux et al. 1999, ²: Veilleux et al. 1995, ³: Duc et al. 1997, ⁴: Iwasawa et al. 2005, ⁵: Severgnini et al. 2001, ⁶: Franceschini et al. 2003, ⁷: Balestra et al. 2005, ⁸: Vignati et al. 1999, ⁹: Imanishi et al. 2003, ¹⁰: Imanishi et al. 2006, ¹¹: Risaliti et al. 2006, ¹²: Sani et al. 2007. †: Sources with simultaneous $\alpha_{bol} > 0.2$ and $\tau > 1$.

Source	α_6	τ	α_{bol}	<i>O/X/L</i>	Source	α_6	τ	α_{bol}	<i>O/X/L</i>
ARP 220	75 \pm 1	1.40 \pm 0.01	9.8 $^{+3.7}_{-2.7}$	L ¹ /SB ⁴ /SB ¹⁰	IRAS 14197+0813	75 \pm 2	2.10 \pm 0.14	10 $^{+5}_{-4}$	-/-/-
IRAS 00091-0738 [†]	90 \pm 1	1.81 \pm 0.04	25 $^{+8}_{-7}$	SB ¹ /-/	IRAS 14252-1550	< 20	< 0.04	< 0.9	L ¹ /-/SB ¹⁰
IRAS 00188-0856	96 \pm 1	0.60 \pm 0.02	45 \pm 9	L ¹ /-/A ^{*10}	IRAS 14348-1447	51 $^{+3}_{-5}$	< 0.09	3.7 $^{+2.1}_{-1.5}$	L ¹ /-/SB ¹¹
IRAS 00456-2904	< 1.0	0	< 0.04	SB ¹ /-/	IRAS 15130-1958	91 $^{+1}_{-3}$	< 0.01	28 $^{+9}_{-11}$	A ¹ /-/A ¹⁰
IRAS 00482-2721	< 54	< 0.04	< 4.1	L ¹ /-/	IRAS 15206+3342	52 \pm 1	0.30 \pm 0.02	3.9 $^{+1.7}_{-1.2}$	SB ¹ /-/SB ¹⁰
IRAS 01003-2238 [†]	96 \pm 1	1.58 \pm 0.02	49 \pm 9	SB ¹ /-/	IRAS 15225+2350	89 \pm 1	0.77 \pm 0.02	22 $^{+7}_{-6}$	SB ¹ /-/SB ¹⁰
IRAS 01166-0844	87 \pm 1	1.19 \pm 0.06	20 $^{+7}_{-6}$	SB ¹ /-/	IRAS 15250+3609	94 \pm 1	0.91 \pm 0.01	35 $^{+9}_{-10}$	L ² /SB ⁶ /-
IRAS 01298-0744 [†]	98 \pm 1	1.79 \pm 0.02	74 $^{+8}_{-9}$	SB ¹ /-/	IRAS 15462-0450	90 $^{+1}_{-16}$	< 0.01	25 $^{+8}_{-18}$	A ¹ /-/
IRAS 01569-2939	85 \pm 1	1.13 \pm 0.04	17 $^{+6}_{-5}$	SB ¹ /-/	IRAS 16090-0139	89 \pm 1	0.69 \pm 0.01	23 $^{+7}_{-6}$	L ¹ /-/A ^{*10}
IRAS 02411+0353	< 17	< 0.01	< 0.8	SB ¹ /-/	IRAS 16156+0146	90 \pm 1	0.37 \pm 0.01	25 $^{+8}_{-6}$	A ¹ /-/
IRAS 03250+1606	< 3.4	< 0.11	< 0.2	L ¹ /-/A ^{*10}	IRAS 16468+5200	85 \pm 1	0.77 \pm 0.02	18 $^{+5}_{-5}$	L ¹ /-/SB ¹⁰
IRAS 04103-2838	56 \pm 1	0.08 \pm 0.02	4.5 $^{+2.0}_{-1.4}$	L ¹ /-/	IRAS 16474+3430	< 4.9	< 0.01	< 0.2	SB ¹ /-/A ^{*10}
IRAS 05189-2524	91 $^{+1}_{-4}$	< 0.01	28 $^{+8}_{-12}$	A ¹ /A ⁵ /A ¹²	IRAS 16487+5447	21 \pm 1	< 0.04	1.0 $^{+0.5}_{-0.4}$	L ¹ /-/A ^{*10}
IRAS 08572+3915	99 \pm 1	0.44 \pm 0.01	85 $^{+5}_{-6}$	L ¹ /-/A ¹⁰	IRAS 17028+5817	< 1.2	0	< 0.05	L ¹ /-/A ^{*10}
IRAS 09039+0503	61 \pm 1	0.71 \pm 0.04	5.5 $^{+2.5}_{-1.7}$	L ¹ /-/A ^{*10}	IRAS 17044+6720	91 \pm 1	0.32 \pm 0.01	26 $^{+8}_{-6}$	L ¹ /-/A ¹⁰
IRAS 09116+0334	< 1.8	< 0.01	< 0.07	L ¹ /-/A ^{*10}	IRAS 17179+5444	84 \pm 1	0.31 \pm 0.02	16 $^{+6}_{-4}$	A ¹ /-/A ¹⁰
IRAS 09539+0857 [†]	91 \pm 1	1.85 \pm 0.03	27 $^{+8}_{-7}$	L ¹ /-/SB ¹⁰	IRAS 17208-0014	< 7.9	< 0.01	< 0.4	L ³ /SB ⁶ /SB ¹¹
IRAS 10190+1322	< 0.3	0	< 0.02	SB ¹ /-/SB ¹⁰	IRAS 19254-7245	89 \pm 1	0.21 \pm 0.08	23 $^{+9}_{-7}$	A ³ /A ⁶ /A ¹¹
IRAS 10378+1109	73 $^{+1}_{-9}$	< 0.01	9.0 $^{+3.7}_{-3.6}$	L ¹ /-/A ^{*10}	IRAS 20100-4156	86 \pm 1	0.47 \pm 0.02	19 $^{+6}_{-5}$	SB ³ /A ⁶ /SB ¹¹
IRAS 10485-1447	60 \pm 1	0.16 \pm 0.03	5.3 $^{+2.4}_{-1.7}$	L ¹ /-/A ^{*10}	IRAS 20414-1651	< 2.2	< 0.07	< 0.09	SB ¹ /-/SB ¹⁰
IRAS 10494+4424	< 0.4	0	< 0.02	L ¹ /-/A ^{*10}	IRAS 20551-4250 [†]	90 \pm 1	1.19 \pm 0.01	25 $^{+8}_{-6}$	L ³ /A ⁶ /A ¹²
IRAS 11095-0238 [†]	94 \pm 1	1.22 \pm 0.01	35 $^{+9}_{-8}$	L ¹ /-/SB ¹⁰	IRAS 21208-0519	< 0.9	0	< 0.04	SB ¹ /-/SB ¹⁰
IRAS 11130-2659	84 \pm 1	1.15 \pm 0.02	16 $^{+6}_{-5}$	L ¹ /-/	IRAS 21219-1757	99 $^{+1}_{-4}$	< 0.01	83 $^{+13}_{-48}$	A ¹ /-/A ¹⁰
IRAS 11387+4116	< 0.8	0	< 0.03	SB ¹ /-/SB ¹⁰	IRAS 21329-2346	43 \pm 2	< 0.07	2.7 $^{+1.3}_{-0.9}$	L ¹ /-/A ^{*10}
IRAS 11506+1331	54 $^{+1}_{-21}$	< 0.01	4.2 $^{+1.9}_{-2.9}$	SB ¹ /-/A ^{*10}	IRAS 22206-2715	< 9.3	< 0.17	< 0.4	SB ¹ /-/
IRAS 12072-0444 [†]	94 \pm 1	1.06 \pm 0.01	37 $^{+9}_{-8}$	A ¹ /-/A ¹⁰	IRAS 22491-1808	< 1.4	0	< 0.06	SB ¹ /SB ⁶ /-
IRAS 12112+0305	< 22	< 0.02	< 1.0	L ¹ /SB ⁶ /SB ¹¹	IRAS 23128-5919	48 \pm 1	0.36 \pm 0.03	3.4 $^{+1.5}_{-1.0}$	L ³ /A ⁶ /A ¹¹
IRAS 12127-1412	98 \pm 1	0.24 \pm 0.08	60 $^{+15}_{-14}$	L ¹ /-/A ¹⁰	IRAS 23234+0946	30 $^{+2}_{-3}$	< 0.05	1.6 $^{+0.8}_{-0.6}$	L ¹ /-/SB ¹⁰
IRAS 12359-0725	54 $^{+2}_{-43}$	< 0.01	4.2 $^{+2.2}_{-3.9}$	L ¹ /-/A ^{*10}	IRAS 23327+2913	73 \pm 1	0.86 \pm 0.03	9.1 $^{+3.8}_{-2.7}$	L ¹ /-/SB ¹⁰
IRAS 13335-2612	< 0.6	0	< 0.02	L ¹ /-/	MRK 231	93 \pm 1	< 0.12	32 $^{+8}_{-7}$	A ¹ /A ⁶ /A ¹⁰
IRAS 13454-2956	59 $^{+1}_{-28}$	< 0.01	5.0 $^{+2.2}_{-3.8}$	A ¹ /-/	MRK 273	67 $^{+1}_{-4}$	< 0.01	7.0 $^{+2.8}_{-2.7}$	A ¹ /A ⁷ /A ¹⁰
IRAS 13509+0442	< 0.6	0	< 0.03	SB ¹ /-/SB ¹⁰	NGC 6240	65 $^{+6}_{-8}$	0.64 \pm 0.24	6.5 $^{+4.8}_{-3.1}$	L ² /A ⁸ /A ¹²
IRAS 13539+2920	< 0.4	0	< 0.02	SB ¹ /-/SB ¹⁰	4C +12.50	97 \pm 1	0.24 \pm 0.02	59 $^{+10}_{-11}$	A ¹ /-/
IRAS 14060+2919	< 0.4	0	< 0.02	SB ¹ /-/SB ¹⁰	UGC 5101 [†]	92 \pm 1	1.09 \pm 0.03	30 $^{+9}_{-8}$	L ² /A ⁹ /A ¹⁰

The results are shown in Fig.3b and prove that our decomposition method is reliable in estimating the AGN/SB contributions both to the 6- μm and to the bolometric luminosity of local ULIRGs. In fact, the estimated 6- μm to bolometric ratios of the SB component in the composite sources (which are located at the bottom right of the plot and are heavily dependent on our modeling) are fully consistent, within the errors, with the ratios of the pure starbursts (located at the bottom left and directly computed from the measured 6- μm and IRAS fluxes). This success is promising in anticipation of a forthcoming study about the role of black hole accretion and star formation in the intense infrared activity characterising the distant galaxies.

However, it is important to keep in mind the main limitations of our approach:

1) The narrow wavelength range used in this work simplifies the decomposition analysis, but prevents us from a complete study of the dust composition, density and geometrical dis-

tribution. These elements strongly affect the overall mid-IR emission longward of the silicate absorption feature, and can be investigated only through an analysis of the whole IRS spectrum.

2) While the 5–8 μm templates seem to have little dispersion (as discussed in detail in Section 3), the spread in the 6- μm to bolometric ratios R^{agn} and R^{sb} can be much higher, making our estimates of the AGN/SB bolometric fractions more uncertain than those in the 5–8 μm band. The uncertainties in α_{bol} reported in Tab.1 are obtained assuming the mean ratios, with the errors on the mean given in Eq.4. However, the dispersion around the best fit in Fig.3a is significantly larger. We therefore consider this dispersion (0.3 dex, constant at all values of α_{bol}) as the actual uncertainty in the bolometric ratios of the individual sources. The numerical results on the individual sources are anyway precise enough to establish which is the dominant source of the observed luminosity.

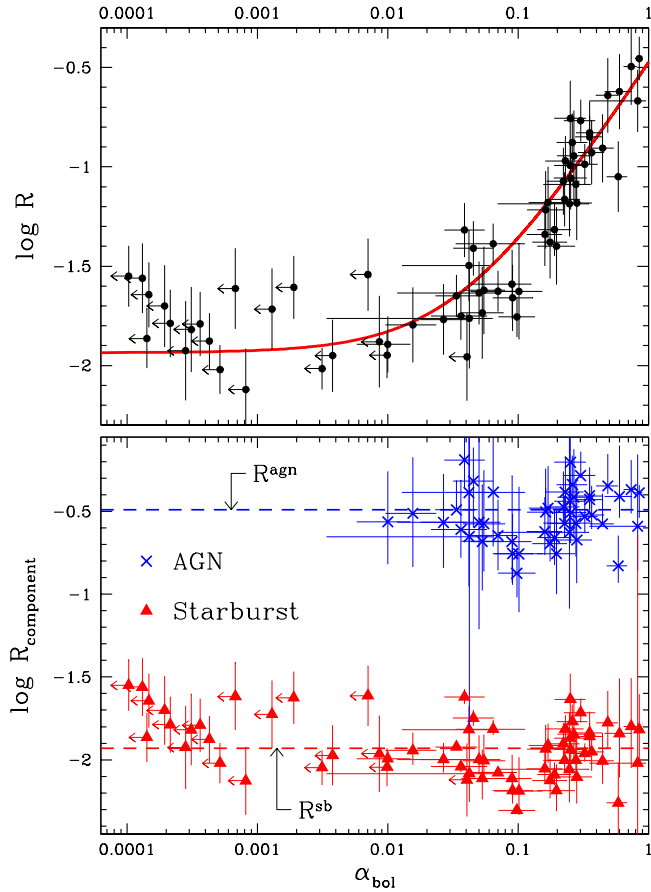


Figure 3. (a) Ratio R between absorption-corrected 6- μ m luminosity and bolometric luminosity, versus the AGN bolometric contribution α_{bol} . The error bars of R are due to the uncertainties in the total infrared flux F_{IR} and in the intrinsic AGN fraction, α_6 . The solid line is the best fit of the R - α_6 relation from Eq.3 (plotted as a function of α_{bol} using Eq.5). (b) Same as above, with the AGN and SB components plotted separately.

Overall, if we consider as a confidence limit the value $\alpha_{bol} = 0.01$ (i.e. the dispersion around our starburst template), an AGN is present in 46 of the 68 ULIRGs in our sample (including several of those optically classified as H II regions), but it is significant ($\alpha_{bol} \gtrsim 0.25$) only in $\sim 30\%$ of the cases. The SB process is responsible for almost 90% of the observed infrared luminosity of ULIRGs, with no significant (i.e. $> 5\%$) bias due to the sample selection. A similar fraction holds for the subsample of 34 sources optically classified as LINERs. Our analysis is also consistent with the findings about the nature of high-redshift infrared-bright galaxies detected in 24 μ m *Spitzer* MIPS surveys. IRS spectroscopy shows that they are mostly $z \sim 1-3$ galaxies, with an apparent bias toward AGN-dominated sources (Houck et al. 2005). This is in agreement with the ~ 30 times higher AGN relative emission in the 5–8 μ m rest-frame wavelength range we have pointed out.

5 CONCLUSIONS

The use of average templates for AGN and SB emission has allowed us to disentangle the two components in the 5–8 μ m

spectra of 68 local ULIRGs, observed with the *Spitzer Space Telescope*. We have been able to detect an AGN in more than 60% of our sources, and estimate its contribution to the bolometric luminosity. In a statistical sense, we confirm that local Ultraluminous Infrared Galaxies are powered for $\sim 85\%$ by intense star formation and for the remaining $\sim 15\%$ by AGN activity. Our method proves to be successful in unveiling an intrinsically faint or obscured AGN inside a ULIRG. In this context we also put on a sound basis our initial assumption that the wavelength interval 5–8 μ m is an appropriate spectral range in order to search for AGNs: an AGN turns out to be approximately 30 times more luminous at 6 μ m than a starburst with the same bolometric luminosity.

ACKNOWLEDGMENTS

We are grateful to the anonymous referee for his/her helpful and constructive comments. We acknowledge financial support from the prin-miur 2006025203 grant and the ASI-NAF grant I/023/05/0.

REFERENCES

- Armus L., et al., 2006, ApJ, 640, 204
- Armus L., et al., 2007, ApJ, 656, 148
- Balestra I., Boller T., Gallo L., Lutz D., Hess S., 2005, A&A, 442, 469
- Brandl B. R., et al., 2006, ApJ, 653, 1129 (B06)
- Draine B. T., 1989, ESASP, 290, 93
- Duc P.-A., Mirabel I. F., Maza J., 1997, A&AS, 124, 533
- Elvis M., et al., 1994, ApJS, 95, 1
- Franceschini A., et al., 2003, MNRAS, 343, 1181
- Genzel R., et al., 1998, ApJ, 498, 579
- Houck J. R., et al., 2004, ApJS, 154, 18
- Houck J. R., et al., 2005, ApJ, 622, L105
- Imanishi M., Terashima Y., Anabuki N., Nakagawa T., 2003, ApJ, 596, L167
- Imanishi M., Dudley C. C., Maloney P. R., 2006, ApJ, 637, 114
- Imanishi M., Dudley C. C., Maiolino R., Maloney P. R., Nakagawa T., Risaliti G., 2007, ApJS, 171, 72
- Iwasawa K., Sanders D. B., Evans A. S., Trentham N., Miniutti G., Spoon H. W. W., 2005, MNRAS, 357, 565
- Kim D.-C., Sanders D. B., 1998, ApJS, 119, 41
- Laurent O., Mirabel I. F., Charmandaris V., Gallais P., Madden S. C., Sauvage M., Vigroux L., Cesarsky C., 2000, A&A, 359, 887
- Netzer H., et al., 2007, ApJ, 666, 806
- Risaliti G., et al., 2006, MNRAS, 365, 303 (R06)
- Sanders D. B., Mirabel I. F., 1996, ARA&A, 34, 749
- Sani E., et al., 2007, arXiv, 709, arXiv:0709.1344
- Severgnini P., Risaliti G., Marconi A., Maiolino R., Salvati M., 2001, A&A, 368, 44
- Spoon H. W. W., Marshall J. A., Houck J. R., Elitzur M., Hao L., Armus L., Brandl B. R., Charmandaris V., 2007, ApJ, 654, L49
- Veilleux S., Kim D.-C., Sanders D. B., Mazzarella J. M., Soifer B. T., 1995, ApJS, 98, 171
- Veilleux S., Kim D.-C., Sanders D. B., 1999, ApJ, 522, 113
- Vignati P., et al., 1999, A&A, 349, L57